The rise of the ruling reptiles and ecosystem recovery from the Permo-Triassic mass extinction

Ezcurra, Martin; Butler, Richard

DOI:
10.1098/rspb.2018.0361

SUPPLEMENTARY INFORMATION

The rise of the ruling reptiles and ecosystem recovery from the Permian-Triassic mass extinction

Martín D. Ezcurra and Richard J. Butler

Corresponding authors emails: martindezcurra@yahoo.com.ar; r.butler.1@bham.ac.uk

Outline of contents

7. Key to silhouettes used in figures 1 and 3

8. References for supplementary information

1. Institutional abbreviations

BIRUG, Lapworth Museum of Geology, University of Birmingham, Birmingham, UK; **CRILAR-Pv**, Centro Regional de Investigaciones y Transferencia Tecnológica de La Rioja, Paleontología de Vertebrados, Anillaco, La Rioja, Argentina; **GPIT**, Paläontologische Sammlung der Universität Tübingen, Tübingen, Germany; **GSI**, Geological Survey of India, Kolkata, India; **GZG**, Geowissenschaftliches Zentrum der Universität Göttingen, Göttingen, Germany; **ISI**, Indian Statistical Institute, Kolkata, India; **IVPP**, Institute of Vertebrate Paleontology and Paleoanthropology, Beijing, China; **MACN-Pv**, Museo Argentino de Ciencias Naturales "Bernardino Rivadavia", Paleovertebrados, Buenos Aires, Argentina; **NHMUK PV**, The Natural History Museum, Palaeontology Vertebrates, London, UK; **NMQR**, National Museum, Bloemfontein, South Africa; **PIN**, Paleontological Institute of the Russian Academy of Sciences, Moscow, Russia; **PULR**, Paleontología, Universidad Nacional de La Rioja, La Rioja, Argentina; **PVL**, Paleontología de Vertebrados, Instituto 'Miguel Lillo', San Miguel de Tucumán, Argentina; **SIDMMG**, Sidmouth Museum, Sidmouth, United Kingdom; **SMNS**, Staatliches Museum für Naturkunde Stuttgart, Stuttgart, Germany; **UNIPAMPA**, Universidade Federal do Pampa, São Gabriel, Brazil; **WARMS**, Warwickshire Museum, Warwick, UK; **ZPAL**, Institute of Paleobiology of the Polish Academy of Sciences, Warsaw, Poland.

2. Taxon-character data matrix and time-bins

(a) Data matrix

The taxon-character data matrix built here is an expansion of that of Ezcurra (2016) and its subsequent modifications (Ezcurra et al., 2017; Nesbitt et al., 2017; Sengupta et al., 2017; Stocker et al., 2017), sampling all 108 currently taxonomically valid middle Permian–early Late Triassic archosauromorph species as well as some unnamed taxa that likely represent distinct species (e.g. the 'Moenkopi poposauroid', the 'Chañares rhynchosaur', NMQR 3570, the 'Waldhaus poposauroid') (supplementary data 3). The scorings of the complete hypodigm of *Archosaurus rossicus* are based on the holotype plus three anterior–middle cervical vertebrae [PIN 1100/66, 66a, 66b], left dentary [PIN 1100/78], skull roof [PIN 1100/84], and three tooth crowns [PIN 1100/85, 85a, 85b]. The scorings of *Lewisuchus admixtus* were modified after considering the referred specimens of "*Pseudolagosuchus major*" as referable to the former species (Arcucci, 1997; Nesbitt et al., 2010; Novas et al., 2015). As a result, the scorings of *Lewisuchus admixtus* are based now on the holotype of the species (PULR 01), the formerly referred specimens of "*Pseudolagosuchus major*" (PULR 053, PVL 3454−3456, MACN-Pv 18954), and a new partial skeleton (CRILAR-Pv 552). Most of the terminals added here were scored based on first hand observations of the specimens, but in some cases, alternatively, published literature was used (for a detailed list of the source of scorings see supplementary table 1). Character 119 was deactivated a priori following Ezcurra et al. (2017), but is maintained in the character list to keep the original character enumeration of Ezcurra (2016).

It should be noted that this data matrix was not built for the purpose of testing phylogenetic relationships, but instead to sample the morphological diversity of middle

Permian−early Carnian archosauromorphs through discrete character-states. The taxon sampling of the dataset was considerably increased in comparison to earlier versions of the matrix (e.g. Nesbitt et al., 2017; Ezcurra et al., 2017; Sengupta et al., 2017), but the terminals were selected because of their age rather than with the objective of reconstructing the phylogenetic relationships among taxa. For example, no late Carnian−Norian poposauroid, lagerpetid, or hyperodapedontine rhynchosaur species were included in the data set and the absence of such deeply nested and morphologically distinctive taxa may result in incorrect character optimizations, such as the optimization of character-states distributed along the most basal branches of a clade as synapomorphies rather than symplesiomorphies. As a result, we do not recommend that the data matrix used here is used to test phylogenetic relationships; instead we recommend use of the version built by Ezcurra (2016) and its subsequent modifications (Ezcurra et al., 2017; Nesbitt et al., 2017; Sengupta et al., 2017; Stocker et al., 2017).

The following scorings were modified from the data set of Ezcurra (2016) and/or its subsequent modifications:

- Character 2. First state expanded to 0.18−0.38.

- *Lewisuchus admixtus*

Multiple scorings were modified because specimens formerly referred to *Pseudolagosuchus major* (MACN-Pv 18954, PULR 053, PVL 3454, 3455, 3456) and a new partial skeleton (CRILAR-Pv 552) were included in this terminal.

- *Parringtonia gracilis*

Character 63: changed from (0) to (?) because the posterior half of the horizontal ramus of the maxilla is missing in the holotype.

Character 613: changed from (0) to (1).

- *Tasmaniosaurus triassicus*

Character 274: changed from (0) to (?) because the distal end of the posterocentral process of the dentary is damaged and, as a result, its shape cannot be determined confidently.

- *Yarasuchus deccanensis*

Character 489: changed from (2) to (?) because it is not clear which humeri and femora in the bone-bed belong to the same individuals (Sen, 2005).

Supplementary table 1: List of terminals added here to the dataset and sources of scorings.

New added terminals	**Source of scoring**
'Panchet proterosuchid'	Multiple specimens from the Panchet Formation of India (GSI, ISI, NHMUK PV collections); MDE and RJB pers. obs.
Teyujagua paradoxa	UNIPAMPA 653; Pinheiro *et al.*, 2016
NMQR 3570	NMQR 3570; Modesto and Botha-Brink, 2008
Bystrowisuchus flerovi	PIN 1043/1346; Sennikov, 2012
Augustaburiania vatagini	Sennikov, 2011
Ctenosauriscus koeneni	GZG.V.4191; Butler *et al.*, 2011
Vytshegdosuchus zbeshartensis	PIN 3361/134; Sennikov, 1988, 1999
Osmolskina czatkoviensis (complete hypodigm)	ZPAL several specimens; Borsuk-Białynicka and Evans, 2003
Halazhaisuchus qiaoensis	IVPP V6027; Sookias *et al.*, 2014
Tanystropheus haasi	Rieppel, 2001
Dinocephalosaurus orientalis	Li, 2003; Rieppel *et al.*, 2008
Protanystropheus antiquus	SMNS 10110, 16687, 50831; Sennikov, 2011
Trachelosaurus fischeri	University of Halle unnumbered; Broili and Fischer, 1916
'Waldhaus poposauroid'	SMNS 91401−91405; Butler *et al.*, 2011
Hypselorhachis mirabilis	NHMUK PV R16586; Butler *et al.*, 2009
Bromsgroveia walkeri	WARMS G.1, 2, G.3a, b, G.5, G.970; BIRUG 2473; Benton and Gower, 1997; Galton, 2012
Stagonosuchus nyassicus	GPIT/RE/3831, 3832; Gebauer, 2004
Mandasuchus tanyauchen	NHMUK PV R6794; Butler *et al.*, in press
'Otter Sandstone archosaur'	SIDMMG 1 2010, SIDMMG 2 2010, SIDMMG 4 2010; Benton, 2011
Lutungutali sitwensis	Peecook *et al.*, 2013
Nyasasaurus parringtoni	NHMUK R6856; Nesbitt *et al.*, 2012
Pectodens zhenyuensis	Li *et al.*, 2017
Macrocnemus fuyuanensis	Li *et al.*, 2007; Jiang *et al.*, 2011

Macrocnemus obristi	Fraser and Furrer, 2013
Fuyuansaurus acutirostris	Fraser *et al.*, 2013
Litorosuchus somnii	Li *et al.*, 2016
'Moenkopi poposauroid'	Nesbitt, 2005
'Chañares rhynchosaur'	CRILAR-Pv 461, 496, 497; Ezcurra *et al.*, 2014a, 2017
Dagasuchus santacruzensis	Lacerda *et al.*, 2015

(b) Terminal pruning

The original version of the data matrix includes several taxa that are late Carnian or younger in age (e.g. *Simoedosaurus lemoinei*, *Herrerasaurus ischigualastensis*, *Heterodontosaurus tucki*, *Dimorphodon macronyx, Trilophosaurus buettneri*, *Tanystropheus longobardicus*, *Dimorphodon macronyx*, *Aetosauroides scagliai*), and which, as a result, lie outside the time span of interest for our analysis. Similarly, the original data matrix includes some non-archosauromorph diapsids (e.g. *Planocephalosaurus robinsonae*, *Youngina capensis*) that are outside the taxonomic scope of our analysis. Therefore, all non-archosauromorph species and archosauromorphs that occur in late Carnian or younger stratigraphic horizons were pruned before the disparity analyses, resulting in a final dataset of 112 terminals, including 108 named species and four unnamed taxa (see above). However, the stratigraphically younger archosauromorph terminals were retained for the phylogenetic diversity and evolutionary rates calculations because of the effects that the ghost lineages that they generate may have on older time bins (supplementary data 4). Choristoderans were excluded because of their problematic phylogenetic position as either the earliest branching archosauromorphs or as non-archosauromorph neodiapsids.

(c) Terminals occurring in >1 time bin

The biochron of the erythrosuchid genus *Shansisuchus* genuinely appears to span two time bins (Anisian and Ladinian) (Liu and Sullivan, 2017). The specimen (IVPP V 22758) described by Liu & Sullivan (2017) from the Tongchuan Formation of Ladinian age possesses several of the diagnostic character-states proposed by Wang et al. (2013) to diagnose *Shansisuchus shansisuchus*—the most complete and only undoubtedly valid species of the genus—and, as a result, may be referred to this species pending a revision of the taxonomic status of *Shansisuchus kuyeheensis* (we could not study the holotype and only known specimen of this species because it could not be located in its repository in 2013; Ezcurra, 2016). Therefore, *Shansisuchus shansisuchus* was included in both the Anisian and Ladinian in all the analyses in order to sample the presence of the genus *Shansisuchus* in the latter time interval.

(d) Parameters of the data matrices

Complete data matrix

Dimensions: 149 terminals and 688 characters

Proportion of missing data and its standard deviation: 62.43±27.69%

Data matrix including terminals with chronostratigraphic uncertainty and excluding non-archosauromorph and post-early Carnian terminals

Dimensions: 112 terminals and 688 characters

Proportion of missing data and its standard deviation: 67.06±27.21%

Data matrix excluding terminals with chronostratigraphic uncertainty, as well as non-archosauromorph and post-early Carnian terminals

Dimensions: 99 terminals and 688 characters

Proportion of missing data and its standard deviation: 67.14±27.40%

Supplementary table 2: Number of terminals sampled in the analyses including and excluding terminals with chronostratigraphic uncertainty, respectively.

Time bin	**Including terminals with chronostratigraphic uncertainty**	**Excluding terminals with chronostratigraphic uncertainty**
middle–late Permian	4	4
Induan	14	9
Olenekian	21	11
Anisian	54	46
Ladinian–early Carnian	33	30

Supplementary table 3: Percentage of missing data in each time bin including and excluding terminals with chronostratigraphic uncertainty, respectively.

Time bin	**Including terminals with chronostratigraphic uncertainty**	**Excluding terminals with chronostratigraphic uncertainty**
Middle–late Permian	80.70%	80.70%
Induan	67.08%	62.60%
Olenekian	78.06%	81.94%
Anisian	67.42%	68.54%
Ladinian–early Carnian	56.44%	57.90%

3. Phylogenetic analysis and temporal calibrations of the trees

The search strategy was described in detail in the Materials and Methods section and the following characters were considered additive (= ordered): 1, 2, 7, 10, 17, 19−21, 28, 29, 36, 40, 42, 50, 54, 66, 71, 74−76, 122, 127, 146, 153, 156, 157, 171, 176, 177, 187, 202, 221, 227, 263, 266, 278, 279, 283, 324, 327, 331, 337, 345, 351, 352, 354, 361, 365, 370, 377, 379, 387, 398, 410, 424, 430, 435, 446, 448, 454, 458, 460, 463, 470, 472, 478, 482, 483, 485, 489, 490, 504, 510, 516, 529, 537, 546, 552, 556, 557, 567, 569, 571, 574, 581, 582, 588, 648, 652, and 662.

The phylogenetic analysis recovered more than 10,000 most parsimonious trees (MPTs) of 3,704 steps, with a consistency index of 0.2414 and a retention index of 0.6270. The topology of the strict consensus tree (SCT) generated from the sample of 10,000 MPTs (supplementary figure 1; supplementary data 5) possesses several polytomies and a lower resolution than the SCTs of previous iterations of this data matrix (Ezcurra, 2016; Nesbitt et al., 2017; Stocker et al., 2017; Ezcurra et al., 2017; Sengupta et al., 2017). In particular, there are two major polytomies that strongly affect the topology of the SCT: one polytomy includes tanystropheids and their relatives, allokotosaurians, rhynchosaurs, and more derived archosauromorphs, and the other is composed of most archosauriforms, retaining only the monophyly of Aetosauria, Phytosauria, Erpetosuchidae, Proterochampsia, Avemetatarsalia, and the *Litorosuchus*+*Vancleavea* clade.

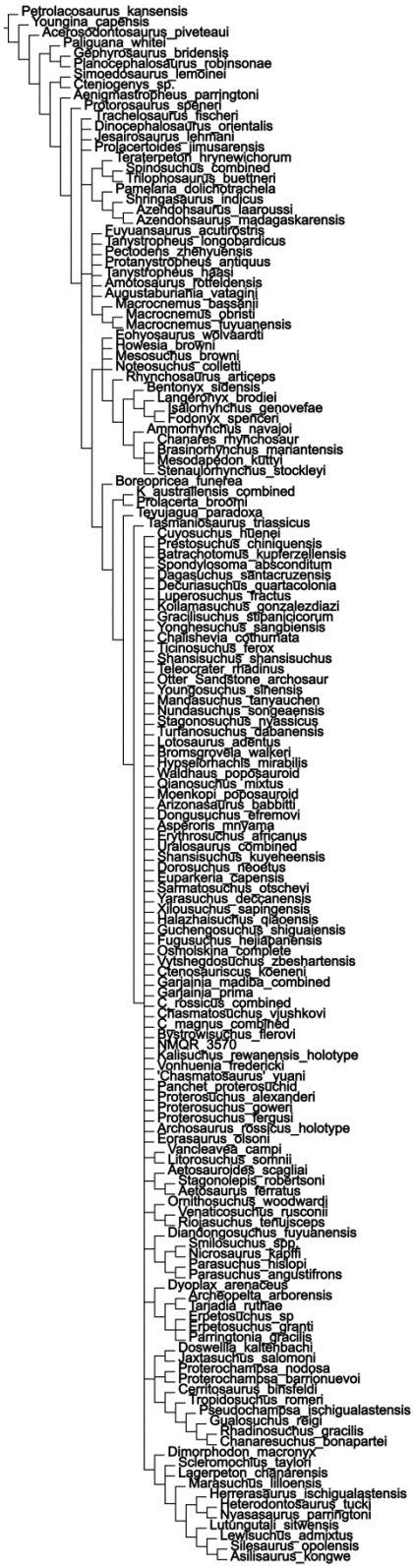

Supplementary figure 1: Strict consensus tree generated from the sample of 10,000 MPTs.

The iterPCR procedure of Pol and Escapa (2009) was used to detect the unstable taxa that cause these major polytomies in the SCT. The iterPCR detected multiple unstable taxa and two iterative a posteriori prunings (removing terminals that resolve more than one node) were conducted in order to recover "moderately resolved" and almost fully resolved strict reduced consensus trees (SRCT). The first "moderately resolved" SRCT (supplementary figure 2) was generated after a posteriori pruning of *Dagasuchus santacruzensis*, the 'Otter Sandstone archosaur', *Vytshegdosuchus zheshartensis*, *Chasmatosuchus rossicus*, *Chasmatosuchus magnus*, "*Chasmatosuchus*" *vjushkovi*, *Bystrowisuchus flerovi*, NMQR 3570, *Eorasaurus olsoni*, and *Prolacertoides jimusarensis*. This SRCT shows good resolution of the main archosauromorph clades and higher-level interrelationships that are congruent with the results of previous analyses of modified versions of this dataset (e.g. Ezcurra *et al.*, 2017; Nesbitt *et al.*, 2017; Sengupta *et al.*, 2017). Some large polytomies remain within the tanystropheid lineage, non-rhynchosaurid and stenaulorhynchine rhynchosaurs, proterosuchids, the closest successive sister taxa of Erythrosuchidae and Eucrocopoda, erythrosuchids, the most basal eucrocopods, and paracrocodylomorph pseudosuchians. An almost fully resolved SRCT (supplementary figure 3) was generated after the pruning of the aforementioned ten terminals plus the following 17 terminals: *Cuyosuchus huenei*, *Batrachotomus kupferzellensis*, *Koilamasuchus gonzalezdiazi*, *Ticinosuchus ferox*, *Youngosuchus sinensis*, *Mandasuchus tanyauchen*, *Bromsgroveia walkeri*, the 'Moenkopi poposauroid', *Asperoris mnyama*, *Uralosaurus magnus*, *Dorosuchus neoetus*, *Xilousuchus sapingensis*, *Halazhaisuchus qiaoensis*, *Kalisuchus rewanensis*, *Vonhuenia friedericki*, *Archosaurus rossicus*, and *Noteosuchus colletti*. The topology of

this SRCT is generally very well resolved and also fully congruent with the results of analyses of previous versions of this data matrix.

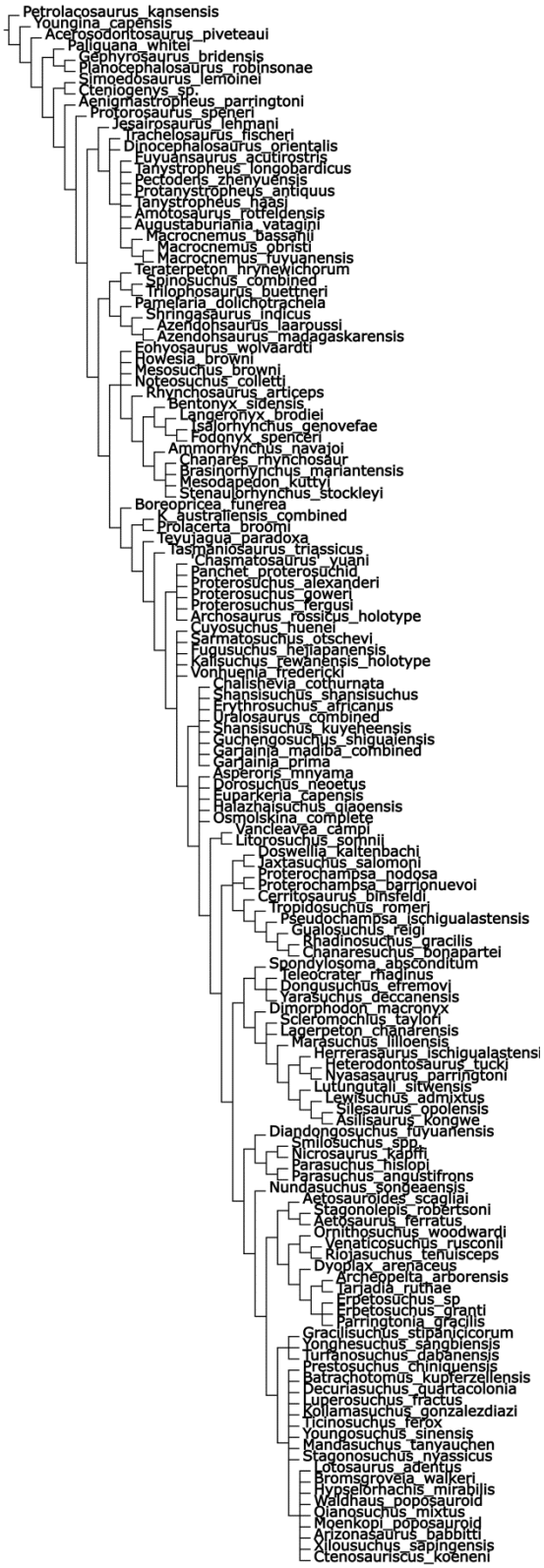

Supplementary figure 2: First SRCT generated from the sample of 10,000 MPTs after the pruning of 10 terminals.

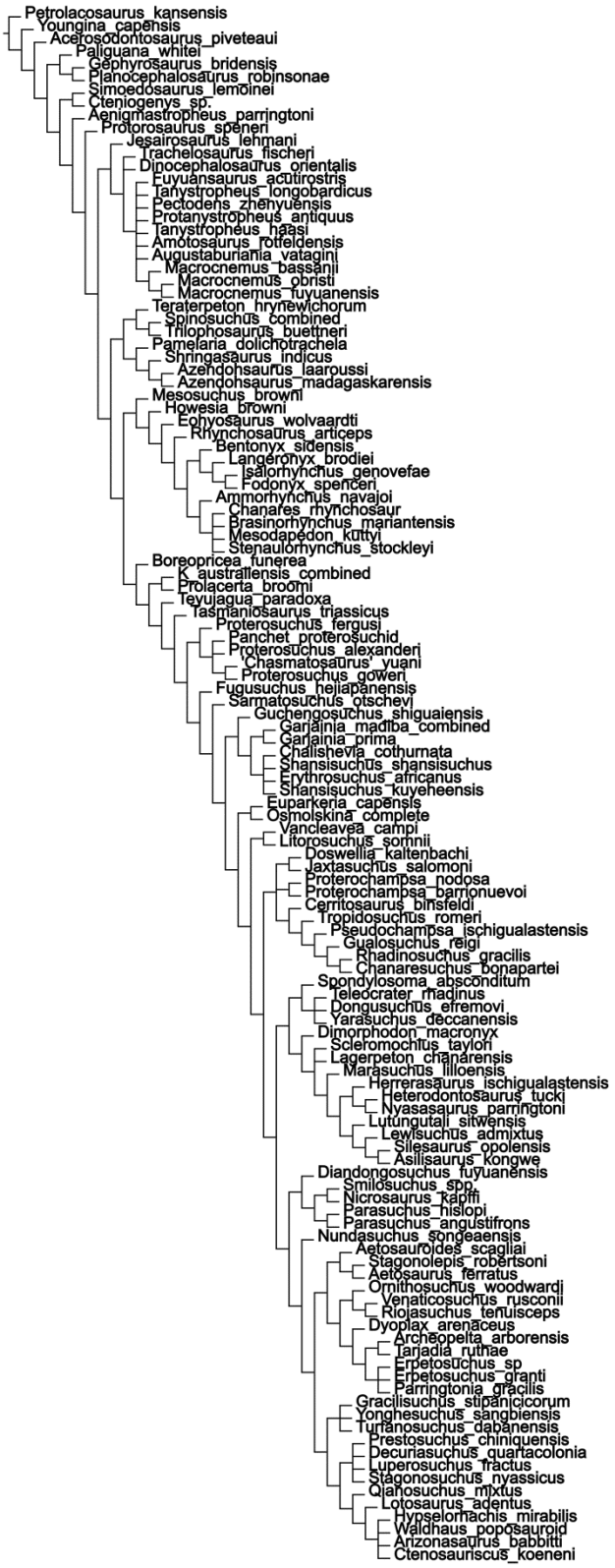

Supplementary figure 3: Second SRCT generated from the sample of 10,000 MPTs after the pruning of 27 terminals.

A random subsample of 100 MPTs were temporally calibrated using the "mbl" method (Laurin, 2004; Brusatte et al., 2008), with a minimum branch length of 0.1 myr and a root age of 269.3 Ma, and used for the main evolutionary rates analysis. Complementary evolutionary rates analyses were conducted using the same calibration settings but with minimum branch lengths of 0.5 myr and 1.0 myr, respectively. In each of these latter analyses a random subsample of 10 temporally calibrated trees were used in order to reduce computational times.

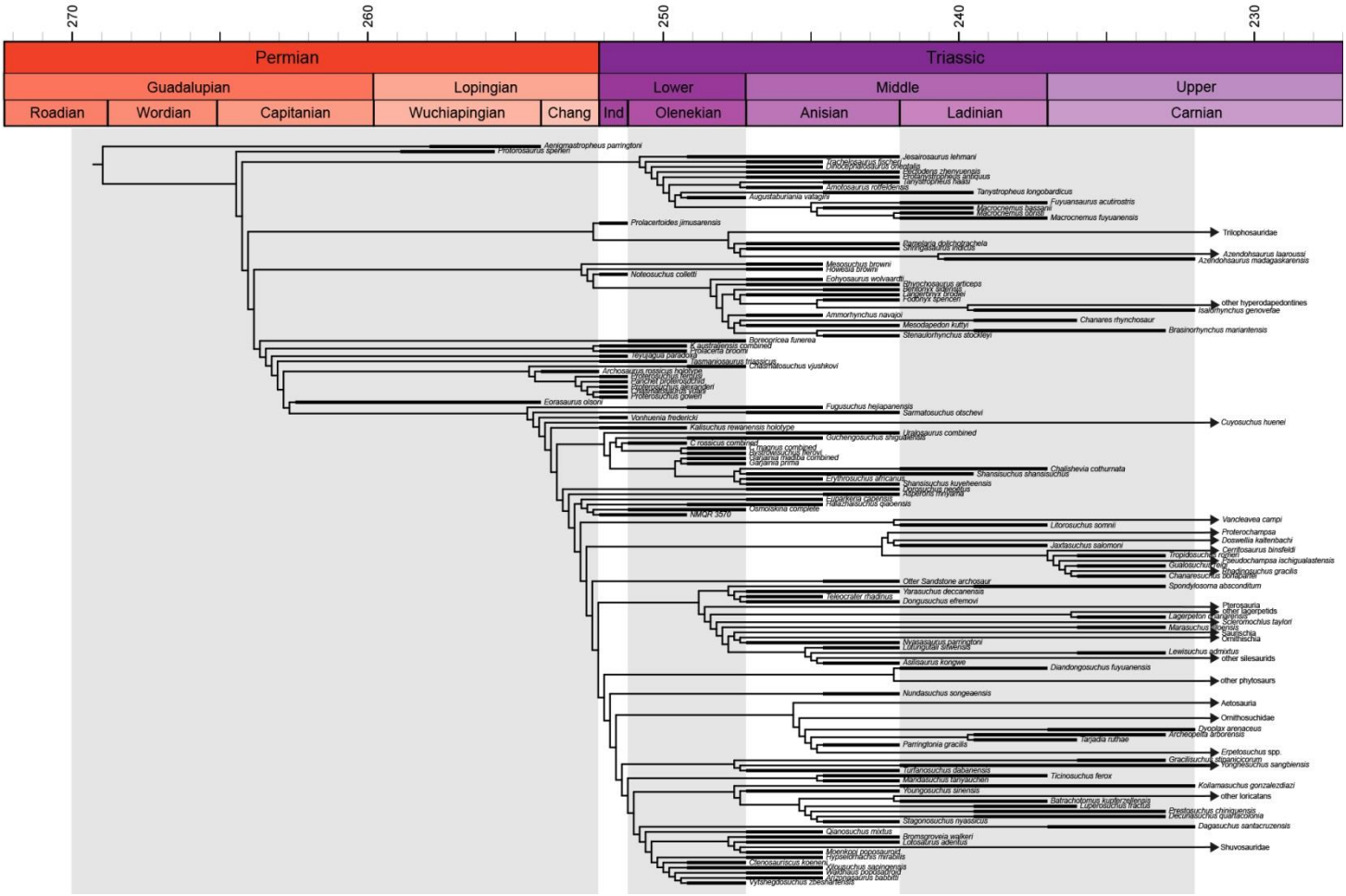

Supplementary figure 4: Example of a time calibrated MPT (minimum branch length of 0.1 myr, randomly selected among all the sampled MPTs). Note that in this tree "other hyperodapedontines", "other lagerpetids", "other loricatans", and "Shuvosauridae" were added by hand using positive monophyletic constrains (see "Phylogenetic diversity"). Branches younger than early Carnian were collapsed and are represented with an arrow.

An additional evolutionary rates sensitivity analysis was conducted using the "cal3" calibration method of Bapst (2013). A set of time bins that equal the shortest intervals of chronostratigraphic uncertainties and possess overlapping ranges (supplementary table 4**)** was created in order to generate ten sampling sets of congruent taxon ranges estimated stochastically from the occurrence data using the `seqTimeList()` function of `palaeotree` (Bapst, 2012) and deactivating the weightSampling option. A value of 0.001 myr was added to the FADs and removed from the LADs of each terminal in order to avoid overlap with the boundaries of the time bins, and also to prevent the situation where terminals were wrongly assigned to an older or younger time bin than that in which they actually occur. Five sets of sampling (0.5822477, 0.5822477, 0.5678570, 0.5527619, and 0.2495298) and extinction (0.10258445, 0.10258445, 0.10427546, 0.09738943, and 0.08226771; used as a proxy of speciation rate) rates were calculated using maximum-likelihood estimates based on this data (Foote, 1997) and were used for the "cal3" calibration. A subsample of four MPTs was selected randomly in order to reduce computational time and were time-calibrated with the `cal3TimePaleoPhy()` function, generating three trees per calibration, not allowing the inference of potential ancestor-descendant relationships, setting the root of the trees to a maximum age of 269.3 Ma, and considering branch rates equal to extinction rates. This protocol was repeated for each of the five sets of sampling and extinction rates in order to account for the uncertainty in these estimated rates, resulting in a total of 60 time-calibrated trees that were used for the evolutionary rates analysis.

Supplementary table 4: Set of time bins used to generate the sampling sets with the function `seqTimeList()`.

Time bin	Lower bound	Upper bound
late Capitanian–Wuchiapingian	262.45	254.14
middle Wuchiapingian	258.90	255.70
middle–late Wuchiapingian	257.91	254.14
Changsinghian	254.14	252.17
Induan	252.17	251.20
early Olenekian	251.20	249.20
late Olenekian–early Anisian	249.20	244.60
late Anisian	244.60	242.00
early Ladinian–late Ladinian	242.00	236.00
late Ladinian	239.50	236.00
early Carnian	236.00	232.00
late Carnian–Aalenian	232.00	170.30

4. Observed species count, phylogenetic diversity estimation, specimen-level abundance data, and archosauromorph-bearing formations

We analyzed patterns of diversity change in the middle Permian−early Carnian archosauromorph record by calculating the following metrics for each of the five time bins.

(a) Observed species count

Represents the raw species count per time bin – this count includes terminals with chronostratigraphic uncertainty (figure 1B; supplementary table 5).

(b) Phylogenetic diversity

This metric represents the number of observed species plus the inferred ghost lineages per time bin (Norell, 1992). Some ghost lineages should be present in our time-calibrated trees based on the results of previous phylogenetic analyses, but they are not recorded because the late Carnian−Norian terminals that produce them are not included in our taxonomic sample which is focused on late Permian−early Carnian taxa (figure 1A). As a result, we included by hand the following four late Carnian−Norian terminals, constraining in TNT 1.5 their monophyly with a specified stratigraphically older taxon, to produce the missing ghost lineages: i) "other hyperodapedontines" constrained as the sister-taxon of *Isalorhynchus* (sensu Montefeltro *et al.*, 2010); ii) "other lagerpetids" constrained as the sister-taxon of *Lagerpeton* (sensu Irmis *et al.*, 2007; Cabreira *et al.*, 2017); iii) "Shuvosauridae" constrained as the sister-taxon of the 'Moenkopi poposauroid' (sensu Nesbitt, 2005); and iv) "other loricatans" constrained as the sister-taxon of *Batrachotomus* (sensu Nesbitt, 2011). The data matrix with these positive monophyletic constraints was analysed using the same tree search strategy described

above. A total of 10,000 MPTs were saved from this analysis and were temporally calibrated using the protocol described above, with a minimum branch length of 0.1 myr (supplementary figure 4). Because the number of ghost lineages that occur per time bin changes with the topology of the tree, we calculated the phylogenetic diversity through time for each of the 10,000 time-calibrated MPTs. Subsequently, a mean phylogenetic diversity with its standard deviation was calculated for each time bin (figure 1C; table 1). Phylogenetic diversity was calculated using a code written for R (R Core Team, 2017) (supplementary data 5).

(c) Specimen-level abundance data

We counted the minimum number of individuals that are currently sampled for each of the middle Permian−early Carnian archosauromorph terminals on the basis of published data and personal observations. We consider different specimens to represent different individuals only if they have overlapping bones. As a result, our estimate is a minimum and is conservative (figure 1C; table 1; supplementary data 2).

(d) Archosauromorph-bearing formations

We counted the number of formations that have yielded currently valid late Permian−early Carnian archosauromorph species on the basis of published data and personal observations (supplementary table 5; supplementary data 2). Formations with chronostratigraphic uncertainty were counted in both time bins.

Supplementary table 5: Observed species count and number of archosauromorph-bearing formations for currently valid late Permian−early Carnian species. Estimated phylogenetic diversity and specimen-level abundance data (number of individuals) are shown in table 1.

Time bin	**Observed species count**	**Archosauromorph-bearing formations**
middle–late Permian	4	4
Induan	14	8
Olenekian	21	14
Anisian	54	23
Ladinian−early Carnian	33	16

The normal distribution of all the variables was tested in R using the function `shapiro.test()` and a normal distribution was not rejected in all cases ($p>0.1$). Comparisons between the above described time series were conducted using generalized least squares (see Materials and Methods). Significant relationships were identified between the time series represented by abundance data, number of archosauromorph-bearing formations and observed species count (supplementary table 6). As a result, these three metrics are not considered as independent from each other in our analyses. By contrast, the time series of phylogenetic diversity was not found to be significantly similar to those of the other metrics.

Supplementary table 6: Results of pairwise comparisons between time series using generalized least squares. Statistically significant results indicated in bold. Estimated phylogenetic diversity and specimen-level abundance data (number of individuals) are shown in table 1.

Comparisons	Slope	t-value	p-value	pseudo-R^2
Abundance ~ Formation counts	17.84	4.88	**0.016**	0.86
Abundance ~ Observed species	7.40	8.62	**0.003**	0.95
Abundance ~ Phylogenetic diversity	1.74	1.03	0.380	0.18
Observed species ~ Formation counts	2.48	11.26	**0.002**	0.97
Observed species ~ Phylogenetic diversity	0.27	1.33	0.276	0.24
Formation counts ~ Phylogenetic diversity	0.130	1.82	0.166	0.39

5. Morphological disparity analyses

Range-based post-ordination (i.e. metrics calculated following a Principal Coordinates Analysis [PCoA]) disparity descriptors (e.g. sum of ranges) are frequently strongly correlated with sample size and amount of missing data. Our dataset possesses highly uneven sample sizes between the five time bins and a relatively high amount of missing data (> 60%) (see above). As a result, we tested the correlation between the amount of missing data in a terminal and its distance from the centroid of the morphospace. We found significant correlations ($p<0.0001$) between these two variables when considering the first 2, 5, 10, 25, 50, 75, and all coordinates of the PCoA generated from the GED dissimilarity matrix (supplementary figure 5). The exclusion of terminals with more than 80% and 70% of missing data still resulted in significant correlations between the amount of missing data and the position of terminals in morphospace when the first two coordinates were considered (80%: $p<0.0001$; 70%: $p=0.0051$), and this correlation was lost only after the pruning the terminals with more than 50% of missing data ($p=0.1842$). However, the exclusion of terminals with more than 50% of missing data resulted in a strongly reduced, non-representative taxon sampling. Similarly, although no significant correlation was recovered between the amount of missing data and the distance of terminals from the centroid, the morphospace generated from the MORD dissimilarity matrix shows some odd features, such as the occurrence of some fragmentary taxa on the periphery of the plot of the first two principal coordinates (25.14% of accumulated variance) (e.g. *Aenigmastropheus parringtoni*, *Tanystropheus haasi*, the 'Chañares rhynchosaur', *Bromsgroveia walkeri*). It is striking that these fragmentary taxa do not occur in positions close to more complete taxa with very

similar scorings (e.g. *Tanystropheus haasi* close to *Tanystropheus longobardicus*, the 'Chañares rhynchosaur' close to *Stenaulorhynchus stockleyi*, *Bromsgroveia walkeri* close to *Arizonasaurus babbitti*). As a result, we decided not to use post-ordination disparity descriptors because they seem to be considerably biased by missing data. Nevertheless, we used the morphospace generated from the PCoA using the GED dissimilarity matrix to show graphically the continuous increase of morphological disparity of archosauromorphs through time (figure 3). The biased position of fragmentary terminals close to the centroid of the morphospace should not affect the general pattern of range expansion in the early evolutionary history of Archosauromorpha because there is no apparent systematic trend in the proportion of missing data through time (supplementary table 3).

By contrast, the pre-ordination disparity metric WMPD (see below) does not show a significant correlation with the proportion of missing data (GED including terminals with chronostratigraphic uncertainty: p=0.0981; MORD including terminals with chronostratigraphic uncertainty: p=0.9787; GED excluding terminals with chronostratigraphic uncertainty: p=0.3170; MORD excluding terminals with chronostratigraphic uncertainty: p=0.6559) or observed species count (GED including terminals with chronostratigraphic uncertainty: p=0.0904; MORD including terminals with chronostratigraphic uncertainty: p=0.4489; GED excluding terminals with chronostratigraphic uncertainty: p=0.0531; MORD excluding terminals with chronostratigraphic uncertainty: p=0.4190) in each time bin, indicating that it is less affected, at least in this dataset, by this bias. The disparity analyses were conducted for the two alternative data sets: that including terminals with chronostratigraphic uncertainty and the other that excludes them. These alternative analyses are aimed at accounting for the sensitivity of the analyses to chronostratigraphic ambiguity of the

sampled terminals. Significant differences between time bins were determined by calculating 95% confidence intervals after 1,000 bootstrap pseudoreplicates of the original data matrix and a recalculation of the dissimilarity matrix and WMPD based on the resampled data sets.

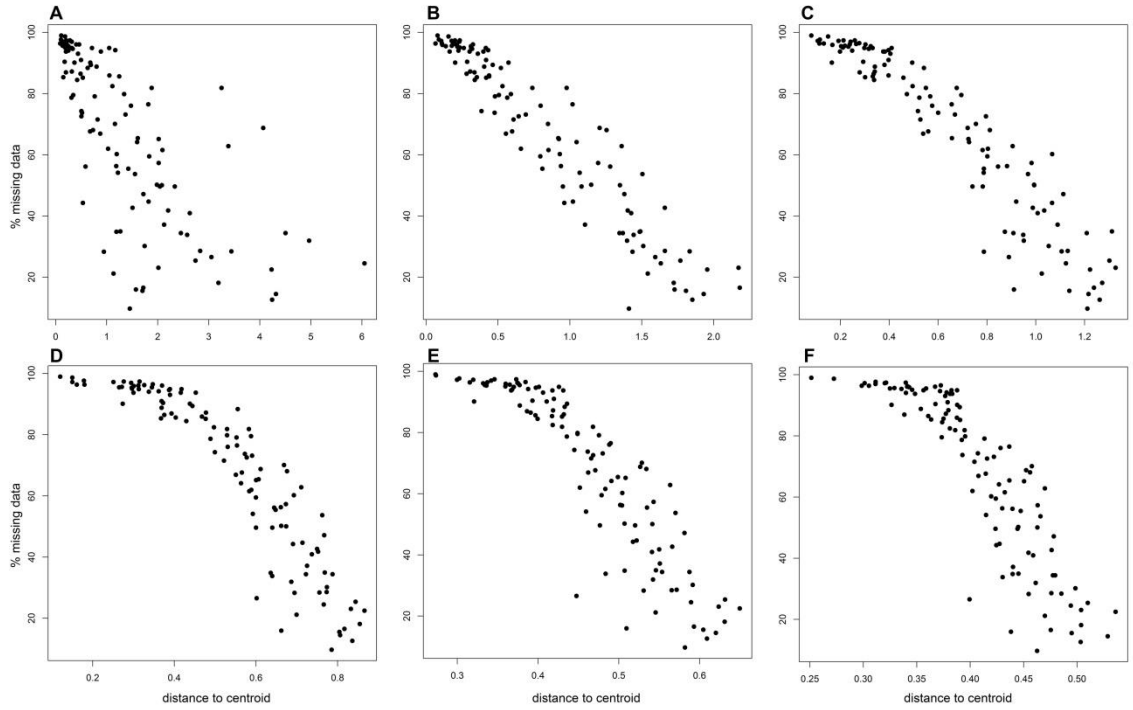

Supplementary figure 5: Bivariate plots of the ratio of missing data of each terminal and its distance to the centroid for the first 2 (A), 10 (B), 25 (C), 50 (D), 75 (E), and all (F) the principal coordinates generated from the GED dissimilarity matrix.

(a) Results including terminals with chronostratigraphic uncertainty

The WMPD values calculated from the GED dissimilarity matrix show a continuous increase of early archosauromorph morphological disparity through time (middle–late Permian to early Carnian) (figure 2B; supplementary figure 6; supplementary table 7). The 95% bootstrapped confidence intervals indicate that the middle–late Permian morphological disparity was significantly lower than in the Olenekian and younger time bins and the Ladinian–early Carnian morphological disparity was significantly higher than in the Olenekian and older time bins.

The WMPD values calculated from the MORD dissimilarity matrix show a pattern of morphological disparity increase through time consistent with that recovered from the GED matrix during the Early, Middle, and early Late Triassic (figure 2; supplementary figure 6; supplementary table 8). In this time span, the Induan morphological disparity is significantly lower than that of younger time bins and the Olenekian disparity is significantly lower than that of the Anisian and Ladinian–early Carnian. The disparity estimates of the latter two time bins do not differ significantly from each other. The results obtained from MORD differ from those recovered from GED in a middle–late Permian WMPD similar and non-significantly different to post-Induan values. However, it should be noted that the 95% bootstrapped confidence interval of the middle–late Permian is remarkably broad, with an upper bound considerable higher than those of the Middle–early Late Triassic and a lower bound that closely approaches the confidence interval of the Induan. Such a broad confidence interval is not unexpected because of the very low archosauromorph sample available during the middle–late Permian (supplementary table 5).

The most striking difference between the WMPD results using the GED and MORD matrices is the presence in the latter of an Induan morphological disparity significantly lower than that of all the other time bins. This result agrees with previous claims of a very low morphological diversity of archosauromorphs during the Induan as a result of the diversity of the group being restricted to proterosuchid-like disaster taxa (Ezcurra and Butler, 2015a). Thus, beyond the different disparity results recovered for the middle–late Permian and Induan, the general pattern of an increase of morphological disparity through time after the Induan is consistent using both dissimilarity matrices.

Supplementary table 7: WMPD results per time bin recovered after the GED dissimilarity matrix and including terminals with chronostratigraphic uncertainty. Bootstrapped WMPD is the mean of the WMPD calculated for each of the pseudoreplicates and lower and upper bounds represent the boundaries of the 95% bootstrapped confidence intervals.

Time bin	WMPD	Bootstrapped WMPD	Lower bound	Upper bound
middle–late Permian	6.743715	6.730356	6.260627	7.211803
Induan	7.346691	7.335081	6.893008	7.790195
Olenekian	8.000208	7.988577	7.540508	8.433184
Anisian	9.375760	9.356068	8.857069	9.863189
Ladinian–early Carnian	10.246279	10.232467	9.702785	10.736783

Supplementary table 8: WMPD results per time bin recovered after the MORD dissimilarity matrix and including two-timer terminals. Bootstrapped WMPD is the mean of the WMPD calculated for each of the pseudoreplicates and lower and upper bounds represents the boundaries of the 95% bootstrapped confidence intervals.

Time bin	WMPD	Bootstrapped WMPD	Lower bound	Upper bound
middle-late Permian	0.4895113	0.4816887	0.3490920	0.6069852
Induan	0.3231418	0.3181848	0.2882402	0.3463113
Olenekian	0.4512585	0.4454826	0.4120701	0.4801130
Anisian	0.5079372	0.5054870	0.4851678	0.5244358
Ladinian-early Carnian	0.5020170	0.5007393	0.4821310	0.5186482

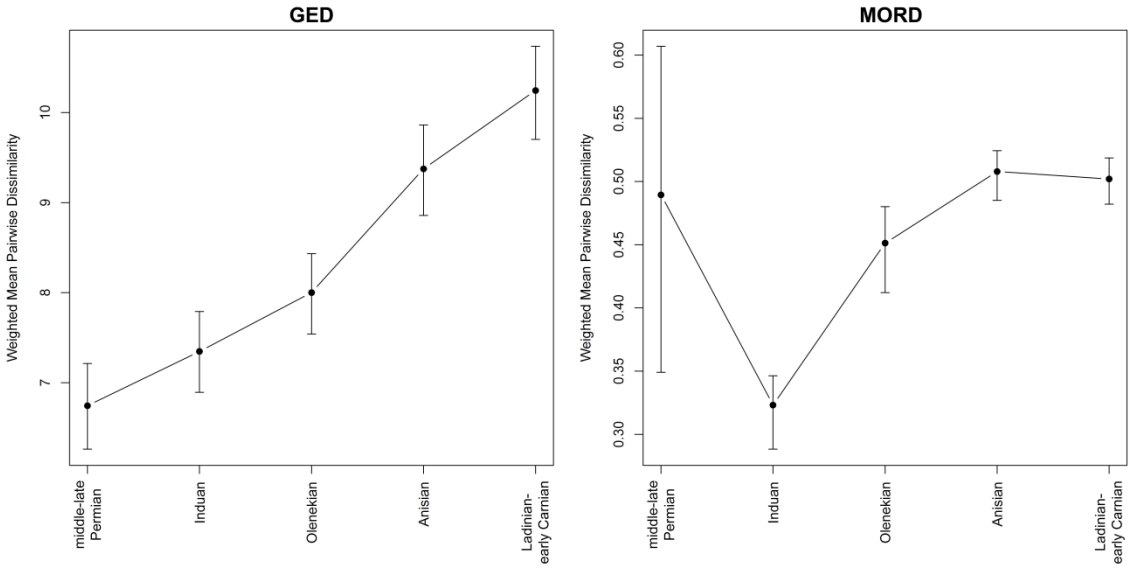

Supplementary figure 6: WMPD values calculated from the GED and MORD dissimilarity matrices, respectively, including terminals with chronostratigraphic uncertainty, plotted through time. Vertical lines represent the 95% bootstrapped confidence intervals.

(b) Results excluding terminals with chronostratigraphic uncertainty

The WMPD patterns through time recovered from the data set excluding terminals with chronostratigraphic uncertainty and using GED or MORD dissimilarity matrices are very similar to that found with the complete data set. The main difference between the results using the GED matrix is the proportionally lower disparity during the Induan and Olenekian after the exclusion of terminals with chronostratigraphic uncertainty (supplementary figure 7; supplementary table 9). As a result, the middle–late Permian, Induan, and Olenekian disparities do not differ from each other, but they are significantly lower than the values recovered for the Anisian and Ladinian–early Carnian. Thus, the disparity curve generated after the exclusion of terminals with chronostratigraphic uncertainty results in a more drastic change in disparity between the Permian−early Middle Triassic and the late Middle Triassic−early Late Triassic time spans. The results recovered from the MORD dissimilarity matrix between the data sets including and excluding terminals with chronostratigraphic uncertainty are very similar to each other, but the Induan disparity is even lower and departs more from the values of the other time-bins (supplementary figure 7; supplementary table 10). In conclusion, the results recovered after the exclusion of terminals with chronostratigraphic uncertainty show that the influence of these taxa on the WMPD disparity metrics are minimal and that they do not modify the general evolutionary patterns recovered here.

Supplementary table 9: WMPD results per time bin recovered after the GED dissimilarity matrix and excluding terminals with chronostratigraphic uncertainty. Bootstrapped WMPD is the mean of the WMPD calculated for each of the pseudoreplicates and lower and upper bounds represent the boundaries of the 95% bootstrapped confidence intervals.

Time bin	WMPD	Bootstrapped WMPD	Lower bound	Upper bound
middle-late Permian	6.743715	6.730356	6.260627	7.211803
Induan	6.658628	6.651397	6.211682	7.083774
Olenekian	7.355798	7.348228	6.847054	7.817243
Anisian	9.383340	9.363134	8.845098	9.894774
Ladinian-early Carnian	10.111620	10.097289	9.564919	10.584896

Supplementary table 10: WMPD results per time bin recovered after the MORD dissimilarity matrix and excluding two-timer terminals. Bootstrapped WMPD is the mean of the WMPD calculated for each of the pseudoreplicates and lower and upper bounds represents the boundaries of the 95% bootstrapped confidence intervals.

Time bin	WMPD	Bootstrapped WMPD	Lower bound	Upper bound
middle-late Permian	0.4895113	0.4816887	0.3490920	0.6069852
Induan	0.2815542	0.2780965	0.2462212	0.3077007
Olenekian	0.4594965	0.4531201	0.4014895	0.5027308
Anisian	0.5090947	0.5065923	0.4854769	0.5262566
Ladinian-early Carnian	0.4986726	0.4974425	0.4783433	0.5169089

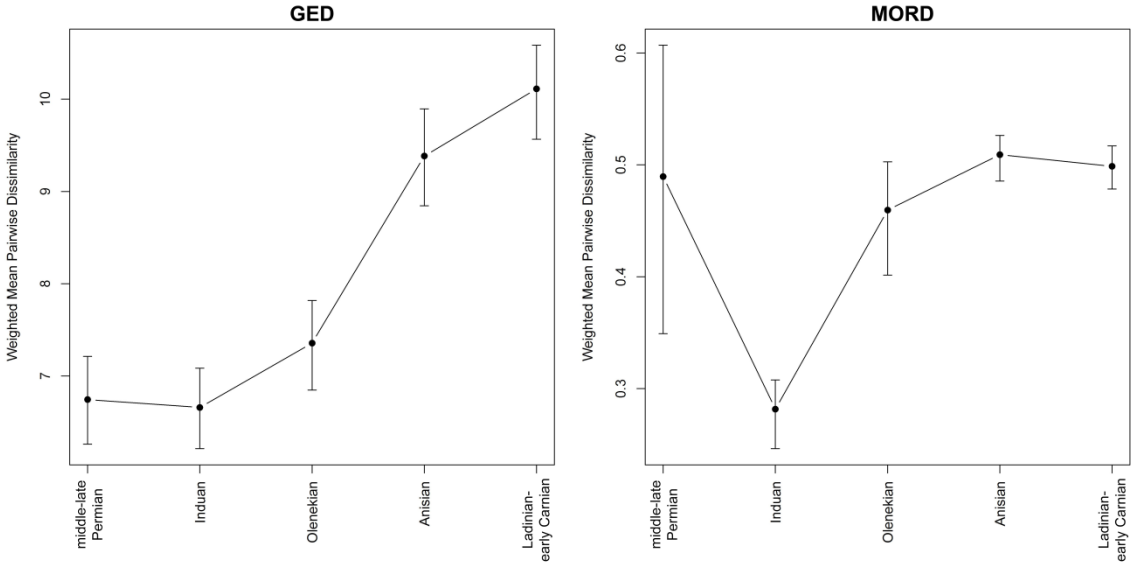

Supplementary figure 7: WMPD values calculated from the GED and MORD dissimilarity matrixes, respectively, excluding terminals with chronostratigraphic uncertainty, plotted through time. Vertical lines represent the 95% bootstrapped confidence intervals.

(c) Results of the modified taxon sampling to equal that of Foth et al. (2016)

The original taxon sampling of our disparity analysis was reduced to equal that of Foth et al. (2016), in which only species for which fairly complete skulls are known were sampled using two-dimensional geometric morphometrics. In addition, the same chronostratigraphic ranges of taxa determined by Foth et al. (2016) were used in this sensitivity analysis. GED and MORD dissimilarity matrices were calculated from this dataset and they were used to calculate WMPD values for the same time bins used by Foth et al. (2016), namely Early Triassic, Anisian, and Ladinian (disparity could not be calculated here for the late Permian because there was only a single species sampled for this time bin: *Protorosaurus speneri*). The WMPD values calculated from both GED and MORD show significant increases of disparity from the Early Triassic to the Anisian and non-significant changes between the Anisian and Ladinian (supplementary tables 11, 12). However, the absolute WMPD value of the Anisian is lower than that of the Ladinian using GED and the opposite occurs using MORD. Thus, these results are fairly consistent with those recovered using the complete data set.

Low archosauromorph disparity around the PT boundary and an increase during the Middle and earliest Late Triassic match the results recovered by Foth et al. (2016), which were based on archosauromorph skulls sampled with two-dimensional geometric morphometrics in lateral view. Foth et al. (2016) found that this pattern was interrupted by a decrease of cranial disparity during the Ladinian, although this decrease was non-significant. A congruent, non-significant, but considerably less conspicuous reduction of archosauromorph disparity is also found here in the Ladinian−early Carnian using MORDdm. We reran our disparity analyses reducing taxon sampling to equal that of Foth et al. (2016), allowing us to generate a more direct comparison between both analyses. These analyses recovered basically the same results as those described above, but the decrease in Ladinian disparity using MORDdm was slightly more conspicuous,

though still non-significant, resembling more closely the results of Foth et al. (2016). These comparisons suggest that disparity analyses based on discretized characters and two-dimensional geometric morphometrics produce similar results for the early archosauromorph radiation, as was previously found for other vertebrate groups (Villier and Eble, 2004; Foth et al., 2012; Hetherington et al., 2015).

Supplementary table 11: WMPD results per time bin recovered from the GED dissimilarity matrix calculated for the reduced dataset that equals that of Foth et al. (2016). Bootstrapped WMPD is the mean of the WMPD calculated for each of the pseudoreplicates and lower and upper bounds represent the boundaries of the 95% bootstrapped confidence intervals.

Time bin	WMPD	Bootstrapped WMPD	Lower bound	Upper bound
middle-late Permian	NA	NA	NA	NA
Early Triassic	9.188211	9.171059	8.602816	9.739448
Anisian	11.667421	11.645882	10.895298	12.472598
Ladinian	12.346640	12.343231	11.672796	13.022914

Supplementary table 12: WMPD results per time bin recovered from the MORD dissimilarity matrix calculated for the reduced dataset that equals that of Foth et al. (2016). Bootstrapped WMPD is the mean of the WMPD calculated for each of the pseudoreplicates and lower and upper bounds represents the boundaries of the 95% bootstrapped confidence intervals.

Time bin	WMPD	Bootstrapped WMPD	Lower bound	Upper bound
middle-late Permian	NA	NA	NA	NA
Early Triassic	0.3723086	0.3709579	0.3441900	0.3967570
Anisian	0.5139368	0.5129762	0.4895383	0.5361311
Ladinian	0.5001818	0.4999518	0.4768739	0.5224676

6. Phenotypic evolutionary rates analyses

Our results show that the evolutionary rates are significantly different ($p<0.0001$) across the time bins and the tree, respectively, in each of the 100 time-calibrated MPTs using a minimum branch length of 0.1 myr. This analysis found that the vast majority of the trees have significantly lower evolutionary rates than the pooled average during the middle–late Permian (mean = 8.76±1.06 character changes per million years), but a few trees possess non-significantly different rates (figure 2A). The Induan evolutionary rates (mean = 16.85±4.52 changes per million years) are not significantly different from the pooled average in most of the MPTs, but several other trees possess significantly higher rates and only one tree shows a significantly low evolutionary rate. The confidence intervals show that the Induan has significantly higher evolutionary rates than the middle–late Permian. Significantly higher evolutionary rates than the pooled average were recovered for all the 100 time-calibrated MPTs in the Olenekian (mean = 20.97±1.27 changes per million years). The Olenekian evolutionary rates are not significantly different from those during the Induan, but this is probably an artefact of the wide range of results recovered among the sampled MPTs in the Induan. Nevertheless, Olenekian rates are significantly higher, with a mean more than twice as high, than those during the middle–late Permian. Anisian evolutionary rates (mean = 11.97±0.46 changes per million years) are significantly lower than those during the Olenekian, marginally non-significantly different than those during the Induan, and significantly higher than those during the middle–late Permian. Anisian evolutionary rates are not significantly different than the pooled average in the vast majority of the MPTs and only a low proportion of them show significantly higher rates. Finally, Ladinian–early Carnian evolutionary rates (mean = 8.27±0.34 changed per million

years) are significantly lower than the pooled average in all MPTs and also significantly lower than the other Triassic time bins, but not significantly different from the rates calculated for the middle–late Permian. The absence of some archosauromorph lineages that are not sampled in our dataset because they do not occur in the fossil record until the late Carnian or later time intervals may result in a underestimation of Ladinian–early Carnian evolutionary rates (e.g. hyperodapedontine rhynchosaurs other than *Isalorhynchus*). However, the vast majority of these younger clades are represented here by at least one of its most informative species (e.g. trilophosaurids, derived doswelliids, some proterochampsids, pterosaurs, dinosaurs, derived silesaurids, derived phytosaurs, aetosaurs, ornithosuchids, derived erpetosuchids) and it seems unlikely that the Ladinian–early Carnian evolutionary rates are strongly underestimated. Thus, we interpret the significantly lower Ladinian–early Carnian evolutionary rates relative to rates in older Triassic time bins as a real biological pattern rather than a sampling artefact.

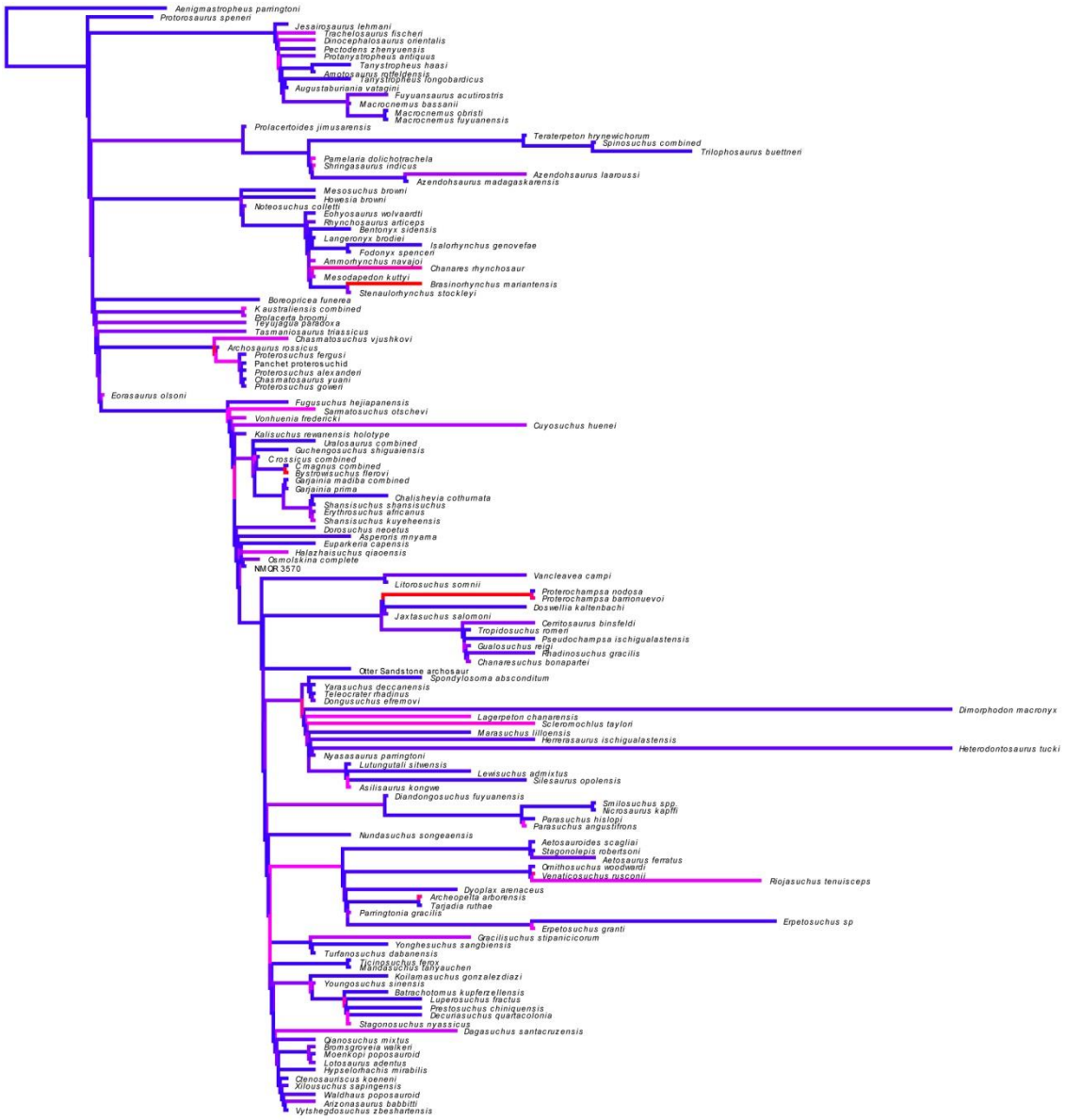

Supplementary figure 8: Randomly selected time-calibrated tree showing evolutionary rates (branch rates) of morphological evolution as a heatmap, in which the values range from 0 (blue) to 481.8 (red).

The analyses of the 10 MPTs time-calibrated using minimum branch lengths of 0.5 and 1.0 myr, respectively, found a similar general pattern that that described above (supplementary figure 8; supplementary table 13). Induan and Olenekian evolutionary rates are significantly higher than those during the middle–late Permian and later Triassic time bins, but no significant difference occurs between these two Early Triassic time bins.

Supplementary table 13: Mean values and standard deviation of the additional evolutionary rates analyses for each time bin. Evolutionary rate values that significantly different from those of the previous time bin are shown in bold.

Time bins	Minimum branch length 0.5 myr	Minimum branch length 1.0 myr	cal3 calibration
late Permian	6.687±0.944	4.469±0.391	7.459±0.702
Induan	**12.877±1.693**	**8.241±0.805**	7.103±0.941
Olenekian	11.645±0.648	7.661±0.359	**8.636±0.372**
Anisian	**8.738±0.371**	**6.693±0.327**	**7.356±0.308**
Ladinian–early Carnian	**6.459±0.326**	**5.230±0.272**	**4.340±0.183**

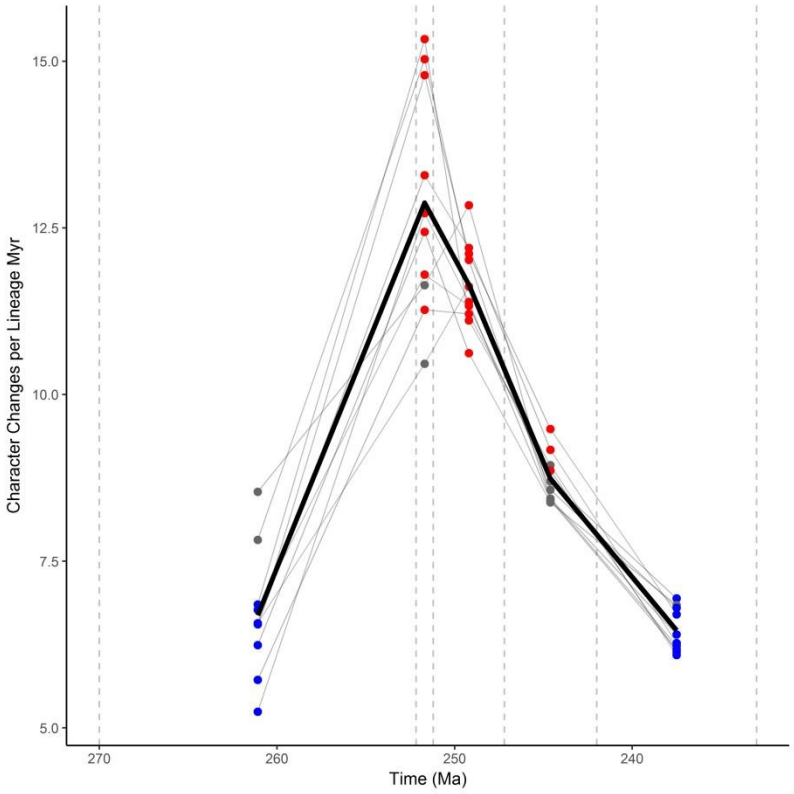

Supplementary figure 9: "Spaghetti" plot showing significantly fast (red) or slow (blue) rates of phenotypic evolution calculated from 10 randomly selected MPTs time-calibrated using a minimum branch length of 0.5 myr. Grey points do not differ significantly from the pooled average rate. Each thin line represents the analysis of one MPT.

The evolutionary rates analysis based on the 60 time-calibrated trees using the "cal3" method recovered mostly the same pattern as the analysis that used the trees calibrated with minimum branch lengths of 0.1 myr. A peak of evolutionary rates is recovered during the Olenekian and significantly lower rates are calculated for the other time bins (supplementary figure 10; supplementary table 13). Most of the Anisian rates are significantly higher than the pooled average, contrasting with the analyses using the "mbl" calibrations, and thus the deceleration of the evolutionary rates is slower using this calibration method. The lowest rates are calculated for the Ladinian−early Carnian, in which most rates are significantly lower than the pooled average. A difference with respect to the analyses using "mbl" calibrations are the relatively high evolutionary rates calculated for the middle–late Permian, in which the mean of the rates is slightly higher, but non-significantly, than that during the Induan. Thus, these alternative analyses show that the key evolutionary rate results recovered here, namely high rates in the Early Triassic and a significant decrease during the Middle and early Late Triassic, are not sensitive to the different temporal calibrations of the MPTs used here.

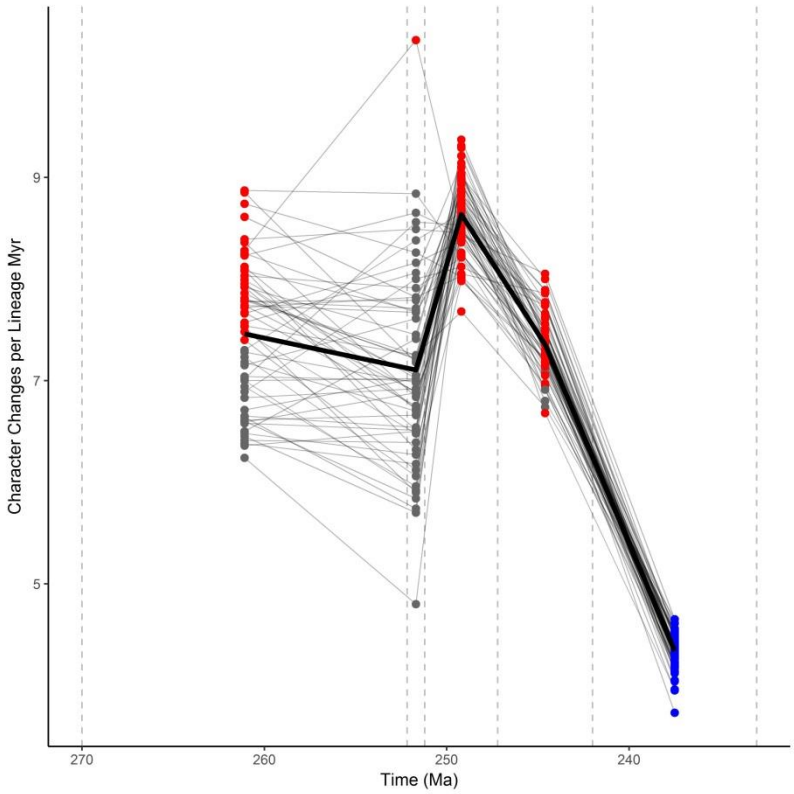

Supplementary figure 10: "Spaghetti" plot showing significantly fast (red) or slow (blue) rates of phenotypic evolution calculated from 60 time-calibrated trees using the "cal3" method. Grey points do not differ significantly from the pooled average rate. Each thin line represents the analysis of one tree.

7. Key to silhouettes used in figures 1 and 3

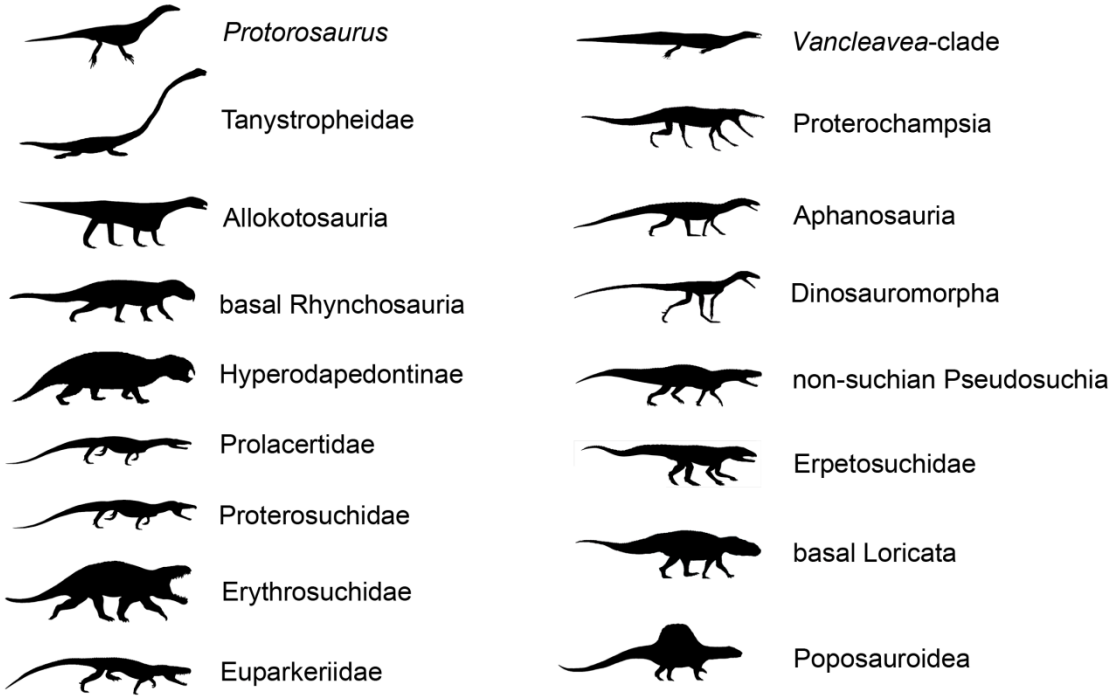

Supplementary figure 11: Explanation of the silhouettes used in figures 1 and 3. Silhouettes taken from Ezcurra and Butler (2015b), Nesbitt et al. (2015, 2017), Li et al. (2016), and Ezcurra et al. (2017).

8. Supplementary references

1. Arcucci AB. 1997 Dinosauromorpha. In *Encyclopedia of Dinosaurs* (eds. Currie PJ, Padian K).San Diego, San Diego Academic Press. pp. 179–183.
2. Bapst DW. 2012 paleotree: an R package for paleontological and phylogenetic analyses of evolution. *Meth. Ecol. Evol.* **3**, 803−807.
3. Bapst DW. 2013 A stochastic rate-calibrated method for time-scaling phylogenies of fossil taxa. *Meth. Ecol. Evol.* **4**, 724−733.
4. Benton MJ. 2011 Archosaur remains from the Otter Sandstone Formation (Middle Triassic, late Anisian) of Devon, southern UK. *Proc. Geol. Ass.* **122**, 25–33.
5. Benton MJ, Gower DJ. 1997 Richard Owen's giant Triassic frogs: archosaurs from the Middle Triassic of England. *J. Vert. Paleontol.* **17**, 74–88.
6. Borsuk-Białynicka M, Evans SE. 2003 A basal archosauriform from the Early Triassic of Poland. *Acta Palaeontol. Pol.* **48**, 649–653.
7. Broili F, Fischer E. 1916 *Trachelosaurus Fischeri* nov. gen. nov. sp. Ein neuer Saurier aus dem Buntsandstein von Bernburg. *Jahrbuch der Koniglichen Preussischen Geologischen Landesanstalt* **37**, 359–414.
8. Brusatte SL, Benton MJ, Ruta M, Lloy GT. 2008 Superiority, competition and opportunism in the evolutionary radiation of dinosaurs. *Science* **321**, 1485−1488.
9. Butler RJ, Barrett PM, Abel RL, Gower DJ. 2009 A possible ctenosauriscid archosaur from the Middle Triassic Manda Beds of Tanzania. *J. Vert. Paleontol.* **29**, 1022–1031.
10. Butler RJ, Brusatte SL, Reich M, Nesbitt SJ, Schoch RR, Hornung JJ. 2011 The sailbacked reptile *Ctenosauriscus* from the latest Early Triassic of Germany and the timing and biogeography of the early archosaur radiation. *PLoS ONE* **6**, e25693.

11. Butler RJ, Nesbitt SJ, Charig AL, Gower DJ, Barrett PM. 2018 *Mandasuchus tanyauchen* gen. et sp. nov., a pseudosuchian archosaur from the Manda Beds (?Middle Triassic) of Tanzania. *Soc. Vert. Paleontol. Mem.* **17**, 96−121.
12. Cabreira SF, Kellner AWA, Dias-da-Silva S, Roberto da Silva L, Bronzati M, Marsola JC, Müller R, Bittencourt J, Batista B, Raugust T, Carrilho R, Brodt A, Langer MC. 2017 A unique Late Triassic dinosauromorph assemblage reveals dinosaur ancestral anatomy and diet. *Curr. Biol.* **26**, 3090–3095.
13. Ezcurra MD. 2016 The phylogenetic relationships of basal archosauromorphs, with an emphasis on the systematic of proterosuchian archosauriforms. *PeerJ* **4**, e1778.
14. Ezcurra MD, Butler RJ. 2015a Taxonomy of the proterosuchid archosauriforms (Diapsida: Archosauromorpha) from the earliest Triassic of South Africa, and implications for the early archosauriform radiation. *Palaeontol.* **58**, 141−170.
15. Ezcurra MD, Butler RJ. 2015b Post-hatchling cranial ontogeny in the Early Triassic diapsid reptile *Proterosuchus fergusi*. *J. Anat.* **5**, 387–402.
16. Ezcurra MD, Trotteyn MJ, Fiorelli LE, Baczko MB von, Taborda JRA, Iberlucea M, Desojo JB. 2014a The oldest rhynchosaur from Argentina: a Middle Triassic rhynchosaurid from the Chañares Formation (Ischigualasto–Villa Unión Basin, La Rioja Province). *Paläontol. Zeits.* **88**, 453–460.
17. Ezcurra MD, Scheyer TM, Butler RJ. 2014b The origin and early evolution of Sauria: reassessing the Permian saurian fossil record and the timing of the crocodile-lizard divergence. *PLoS ONE* **9**, e89165.
18. Ezcurra MD, Fiorelli LE, Martinelli AG, Rocher S, Baczko MB von, Ezpeleta M, Taborda JRA, Hechenleitner EM, Trotteyn MJ, Desojo JB. 2017 Deep faunistic turnovers preceded the raise of dinosaurs in southwestern Pangaea. *Nat. Ecol. Evol.* **1**, 1477–1483.

19. Foote M. 1997 Estimating taxonomic durations and preservation probability. *Paleobiol.* **23**, 278−300.
20. Foth C, Brusatte SL, Butler RJ. 2012 Do different disparity proxies converge on a common signal? Insights from the cranial morphometrics and evolutionary history of Pterosauria (Diapsida: Archosauria). *J. Evol. Biol.* **25**, 904–915.
21. Foth C, Ezcurra MD, Sookias R, Brusatte SL, Butler RJ. 2016 Unappreciated diversification of stem archosaurs during the Middle Triassic predated the dominance of dinosaurs. *BMC Evol. Biol.* **16**, 188.
22. Fraser NC, Furrer H. 2013 A new species of *Macrocnemus* from the Middle Triassic of the eastern Swiss Alps. *Swiss J. Geosc.* **106**, 199–206.
23. Fraser NC, Rieppel O, Li C. 2013 A long-snouted protorosaur from the Middle Triassic of southern China. *J. Vert. Paleontol.* **33**, 1120–1126.
24. Galton PM. 2012 Notes on bones and teeth of *Bromsgroveia* and other archosaurian reptiles from the lower Middle Triassic (Anisian) of the English Midlands. *Rev. Paléobiol.* **31**, 171–204.
25. Gebauer E. 2004 Neubeschreibung von *Stagonosuchus nyassicus* v. Huene, 1938 (Thecodontia, Rauisuchia) aus der Manda-Formation (Mittlere Trias) von Südwest-Tansania. *Neues Jahrb. Geol. Paläontol.* **231**, 1–35.
26. Hetherington AJ, Sherratt E, Ruta M, Wilkinson M, Deline B, Donoghue PCJ. 2015 Do cladistic and morphometric data capture common patterns of morphological disparity? *Palaeontol.* **58**, 393–399.
27. Irmis RB, Nesbitt SJ, Padian K, Smith ND, Turner AH, Woody D, Downs AA. 2007 Late Triassic dinosauromorph assemblage from New Mexico and the rise of dinosaurs. *Science* **317**, 358–361.

28. Jiang DY, Rieppel O, Fraser NC, Motani R, Hao WC, Tintori A, Sun Y-L, Sun ZY. 2011 Skeletal anatomy of *Macrocnemus fuyuanensis* Li et al., 2007, based on a new specimen from the latest Ladinian/earliest Carnian of the Middle/Late Triassic of Southwestern China. *J. Vert. Paleontol.* **31**, 1230–1237.
29. Lacerda MB, Schultz CL, Bertoni-Machado C. 2015 First 'rauisuchian' archosaur (Pseudosuchia, Loricata) for the Middle Triassic *Santacruzodon* Assemblage Zone (Santa Maria Supersequence), Rio Grande do Sul State, Brazil. *PLoS ONE* **10**, e0118563.
30. Laurin M. 2004 The evolution of body size, Cope's Rule and the origin of amniotes. *Syst. Biol.* **53**, 594−622.
31. Li C. 2003 First record of protorosaurid reptile (Order Protorosauria) from the Middle Triassic of China. *Acta Geol. Sin.* **77**, 419–423.
32. Li C, Zhao L-J, Wang L-T. 2007 A new species of *Macrocnemus* (Reptilia: Protorosauria) from the Middle Triassic of southwestern China and its palaeogeographical implication. *Science in China, Series D, Earth Sciences* **50**, 1601–1605.
33. Li C, Wu XC, Zhao LJ, Nesbitt SJ, Stocker MR, Wang LT. 2016 A new armored archosauriform (Diapsida: Archosauromorpha) from the marine Middle Triassic of China, with implications for the diverse life styles of archosauriforms prior to the diversification of Archosauria. *Sci. Nat.* **103**, 95.
34. Li C, Fraser NC, Rieppel O, Zhao LJ, Wang LT. 2017 A new diapsid from the Middle Triassic of southern China. *J. Paleontol.* **91**, 1306–1312.
35. Liu J, Sullivan C. 2017 New discoveries from the *Sinokannemeyeria-Shansisuchus* Assemblage Zone: 3. Archosauriformes from Linxian, Shanxi, China. *Vertebrat. PalAsiatic.* **55**, 110–128.

36. Modesto SP, Botha-Brink J. 2008 Evidence of a second, large archosauriform reptile in the Lower Triassic Katberg Formation of South Africa. *J. Vert. Paleontol.* **28**, 914–917.
37. Montefeltro FC, Langer MC, Schultz CL. 2010 Cranial anatomy of a new genus of hyperodapedontine rhynchosaur (Diapsida, Archosauromorpha) from the Upper Triassic of Southern Brazil. *Earth Env. Sci. T. R. Soc.* **101**, 27–52.
38. Nesbitt SJ. 2005 A new archosaur from the upper Moenkopi Formation (Middle Triassic) of Arizona and its implications for rauisuchian phylogeny and diversification. *Neues Jahrb. Geol. Paläontol.***6**, 332–346.
39. Nesbitt SJ. 2011 The early evolution of archosaurs: relationships and the origin of major clades. Bull. *Am. Mus. Nat. Hist.* **352**, 1−292.
40. Nesbitt SJ, Sidor CA, Irmis RB, Angielczyk KD, Smith RMH, Tsuji LA. 2010 Ecologically distinct dinosaurian sister-group shows early diversification of Ornithodira. *Nature* **464**, 95−98.
41. Nesbitt SJ, Barrett PM, Werning S, Sidor CA, Charig AJ. 2013 The oldest dinosaur? A Middle Triassic dinosauriform from Tanzania. *Biol. Lett.* **9**, 20120949.
42. Nesbitt SJ, Flynn JJ, Pritchard AC, Parrish JM, Ranivoharimanana L, Wyss AR. 2015 Postcranial osteology of *Azendohsaurus madagaskarensis* (? Middle to Upper Triassic, Isalo Group, Madagascar) and its systematic position among stem archosaur reptiles. *Bull. Am. Mus. Nat. Hist.* **398**, 1–126.
43. Nesbitt SJ, Butler RJ, Ezcurra MD, Barrett PM, Stocker MR, Angielczyk KD, Smith RMH, Sidor CA, Niedźwiedzki G, Sennikov A, Charig AJ. 2017 The earliest bird-line archosaurs and assembly of the dinosaur body plan. *Nature* **544**, 484−487.

44. Norell, M. A. 1992 Taxic origin and temporal diversity: the effect of phylogeny. In *Extinction and Phylogeny* (eds. Novacek MJ, Wheeler QD). New York, Columbia University Press. pp. 88–118.
45. Novas FE, Agnolín FL, Ezcurra MD. 2015 Taxonomy of basal dinosauriforms: evidence provided by a new specimen from the Triassic Chañares Formation, NW Argentina. In *Libro de resúmenes del V Congreso Latinoamericano de Paleontología de Vertebrados*. Montevideo, V CLPV. p. 50.
46. Peecook BR, Sidor CA, Nesbitt SJ, Smith RMH, Steyer JS, Angielczyk KD. 2013 A new silesaurid from the upper Ntawere Formation of Zambia (Middle Triassic) demonstrates the rapid diversification of Silesauridae (Avemetatarsalia, Dinosauriformes). *J. Vert. Paleontol.* **33**, 1127−1137.
47. Pinheiro FL, França MA, Lacerda MB, Butler RJ, Schultz CL. 2016 An exceptional fossil skull from South America and the origins of the archosauriform radiation. *Sci. Rep.* **6**, 22817.
48. Pol D, Escapa IH. 2009 Unstable taxa in cladistic analysis: identification and the assessment of relevant characters. *Cladistics* **25**, 515−527.
49. R Core Team. 2017 *R: a language and environment for statistical computing*. Vienna, Austria: R Foundation for Statistical Computing. See https://www.r-project.org/
50. Rieppel O. 2001 A new species of *Tanystropheus* (Reptilia: Protorosauria) from the Middle Triassic of Makhtesh Ramon, Israel. *Neues Jahrb. Geol. Paläontol.* **221**, 271−287.
51. Rieppel O, Li C, Fraser NC. 2008 The skeletal anatomy of the Triassic protorosaur *Dinocephalosaurus orientalis* Li, from the Middle Triassic of Guizhou Province, southern China. *J. Vert. Paleontol.* **28**, 95−110.

52. Sengupta S, Ezcurra MD, Bandyopadhyay S. 2017 A new horned and long-necked herbivorous stem-archosaur from the Middle Triassic of India. *Sci. Rep.* **7**, 8366.
53. Sennikov AG. 1988 New rauisuchids from the Triassic of European Russia. *Paleontol. J.* **1988**, 124−128.
54. Sennikov AG. 1999 The evolution of the postcranial skeleton in archosaurs in connection with new finds of the Rauisuchidae in the Early Triassic of Russia. *Paleontol. J.* **33**, 648−659.
55. Sennikov AG. 2011 New tanystropheids (Reptilia: Archosauromorpha) from the Triassic of Europe. *Paleontol. J.* **45**, 90−104.
56. Sennikov AG. 2012 The first ctenosauriscid (Reptilia: Archosauromorpha) from the Lower Triassic of eastern Europe. *Paleontol. J.* **46**, 499–511.
57. Sookias RB, Sullivan C, Liu J, Butler RJ. 2014 Systematics of putative euparkeriids (Diapsida: Archosauriformes) from the Triassic of China. *PeerJ* **2**, e658.
58. Stocker MR, Zhao LJ, Nesbitt SJ, Wu XC, Li C. 2017 A short-snouted, Middle Triassic phytosaur and its implications for the morphological evolution and biogeography of Phytosauria. *Sci. Rep.* **7**, 46028.
59. Villier L, Eble GJ. 2004 Assessing the robustness of disparity estimates: the impact of morphometric scheme, temporal scale, and taxonomic level in spatangoid echinoids. *Paleobiol*. **30**, 652–665.